Heliyon 10 (2024) e26396

Contents lists available at ScienceDirect

Heliyon

journal homepage: www.cell.com/heliyon

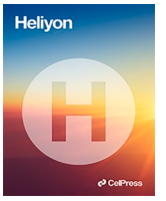

Research article

Enhanced thermal conductivity of plasma generated ZnO–MgO based hybrid nanofluids: An experimental study

Aqsa Nazir [a], Adnan Qamar [b], Muhammad Shahid Rafique [a], Ghulam Murtaza [a], Tehreem Arshad [a], Abdul Muneeb [a], Kanwal Jabeen [c], M.A. Mujtaba [b], H. Fayaz [d,*], C Ahamed Saleel [e]

[a] *Laser and Optronics Centre, Department of Physics, University of Engineering and Technology Lahore, Lahore, 54890, Pakistan*
[b] *Department of Mechanical, Mechatronics and Manufacturing Engineering, New Campus, University of Engineering and Technology Lahore, Lahore, Pakistan*
[c] *Department of Mathematics, University of Engineering and Technology Lahore, Lahore, 54890, Pakistan*
[d] *Modeling Evolutionary Algorithms Simulation and Artificial Intelligence, Faculty of Electrical and Electronics Engineering, Ton Duc Thang University, Ho Chi Minh City, Vietnam*
[e] *Department of Mechanical Engineering, College of Engineering, King Khalid University, Asir-Abha, 61421, Saudi Arabia*

A R T I C L E I N F O

Keywords:
Band gap energy
Hybrid nanofluids
Nanoparticles
Plasma synthesis
Thermal conductivity

A B S T R A C T

Hybrid nanofluids (HNFs) of metallic oxide-based nanoparticles (NPs) have been prepared in different basefluids (BFs) employing the thermal plasma technique. NPs of ZnO–MgO were directly dispersed into pristine coolant, engine oil, distilled water (DW), and coconut oil. Plasma was generated between two identical electrodes applying 8.0 kV at the ambient conditions and proved economically viable in preparing stable HNFs. X-ray Diffractometry (XRD) showed ZnO and MgO NPs possessed hexagonal and cubic crystal structures, respectively. The band gap is calculated through UV-visible spectroscopy. The thermal conductivity (TC) of the HNFs has been measured using a thermal conductivity analyzer based on the transient hot wire method. The band gaps of pristine coolant and its HNFs were obtained to be 3.35 eV and 3.33 eV, respectively. In engine oil and its HNFs, band gaps of 3.16 eV and 3.02 eV have been extracted. There appears to be a slight reduction in band gap for coolant and engine oil-based HNFs. The band gap value of coconut oil-based HNFs was 4.05 eV, which showed a higher value than the pristine coconut oil-based HNFs (3.95 eV). The band gap calculated in the case of DW-based HNFs was 3.79 eV. TC of HNFs with volume concentration of 0.019 % for DW, 0.020 % for coolant, 0.016 % for engine oil, and 0.017 % for coconut oil were tested between 20 and 60 °C. An increase in TC was observed with the rise in temperature of the HNFs. Maximum increment in TC was observed at 60 °C for coolant-based HNFs, which was 19 %, followed by DW (18%), coconut oil (18%), and engine oil (16%), respectively. DW-based HNFs can be used as a coolant and optical filter for optoelectronics devices like photovoltaic cells for better performance. The study underscores precise control of NPs size as pivotal for band gap influence. HNFs hold promise as the next-gen heat transfer fluids (HTFs), revolutionizing thermal conductivity across industries. This research lays a firm foundation for plasma-synthesized HNFs' application in enhanced heat transfer and optoelectronic devices. Coolant-based HNFs excel in thermal conductivity, addressing heat transfer challenges.

* Corresponding author.
E-mail address: fayaz@tdtu.edu.vn (H. Fayaz).

https://doi.org/10.1016/j.heliyon.2024.e26396
Received 23 August 2023; Received in revised form 5 February 2024; Accepted 12 February 2024
Available online 16 February 2024

1. Introduction

Increasing development in science and technology demands enhanced heat transfer in many engineering applications, including but not limited to the cooling of electronic systems [1], automotive engines [2], transformers [3], heat exchangers [4], solar collectors [5], and thermal management of optoelectronic devices [6]. A short time ago, conventional fluids like water, engine oil, mineral oils, and ethylene glycol (EG) were usually used in time-honored ways for cooling these systems [7]. These cooling liquids have a low thermal conductivity (TC) that can reduce the devices' lifetime and affect their performance. This problem has led thermal engineers to consider new techniques and methodologies to resolve the issue. Nanofluids (NFs), newly engineered fluids with superior thermal properties, are comprehensively implemented in many industrial and commercial thermal applications for heat removal with increased performance compared to conventional fluids [8]. NFs containing NPs of two or more dissimilar or different metals or metal oxides are called hybrid nanofluids (HNFs). HNFs are the potential fluids that offer better heat transfer, thermophysical properties, and optical and chemical properties than conventional cooling fluids and NFs with single NPs [9]. Due to synergistic effects, HNFs proved to be more productive cooling fluids for efficient heat transfer for modern equipment and industry [10].

The higher TC of metallic and metal oxide-based NPs could enhance the thermal performance of conventional BFs [11]. The improvement of TC in HNFs depends on many factors, including but not limited to the pH of BFs, viscosity (VC), NPs size, morphology of NPs, and the operating temperature [12]. The fundamental cause for the greater TC of NPs than bulk solids is that NPs have a higher surface area-to-volume ratio than bulk material. Brownian motion of solid NPs into ordinary BFs and nanolayer formation is very much involved in the greater thermal performance of HNFs [13]. Water, EG, and oils have been used to remove heat for many decades, but introducing NPs in these fluids improved their performance, reduced the sizes of heat exchange systems, and minimized fuel consumption. Many researchers have done work on efficiently removing heat from heat exchangers using HNFs that play an important role in industrial machine maintenance [14].

Two methods for preparing HNFs have been discussed in the existing literature. These are the one-step method and the two-step method. The one-step method requires simultaneously the preparation and dispersion of NPs into the BFs. In this method, NPs formed straight into the BFs with uniform dispersion and better stability [15]. Drawbacks of this method include the high cost and not being suitable for extensive production, e.g., laser ablation method, electrical explosion wire (EEW) method, and acetylene flame synthesis system. In the two-step method, NPs are first synthesized as dry powders with the help of mechanical or chemical processes such as ball milling, vapor phase, sol-gel, or grinding. After that, this powder is dispersed into the BFs with an ultrasonic bath, high shear mixing, ultrasonic disruptor, and high-pressure homogenizer to avoid aggregation, which is dominant in this case. This method is time-consuming but can be used at the industrial level with a low cost of production [16]. To enhance the working and lifetime of heat removal devices, Kumar et al. [17] experimentally investigated the thermal performance of Cu: Zn-based HNFs prepared at a concentration of (50:50). They used various BFs (vegetable oil, paraffin oil, and SAE oil) and realized that the HNFs based on vegetable oil exhibited a sharper TC enrichment compared to other two BFs. MWCNT-CuO-SiO_2-based HNFs were tested in aqueous media for their thermal performance. It was investigated that there was a significant rise in the TC of the HNFs and the concentration of NPs, the ratio of each NPs type in the host fluid, and the operating temperature influenced it [18]. In their investigation, Esfe et al. [19] tested MWCNT and TiO_2-based HNFs in different NPs concentration ratios in water-EG-based host BFs. The findings revealed that the water-EG (80:20) based HNFs exhibited enhanced TC compared to water-EG (50:50) based NFs. In another study with the MWCNT and TiO_2-based HNFs, the same authors confirmed that HNFs' TC was also greatly influenced by the ratio of water-EG when the NPs were dispersed in the same concentration. The economic performance indicators also reflected that the former HNFs, with a water-EG ratio of 80:20, possessed a higher price-performance factor, making them suitable for industrial applications [20].

Marulasiddeshi et al. [21] synthesized Al_2O_3 and CuO-based NPs using the sol-gel method and then prepared Al_2O_3–CuO (50:50) HNFs using the standard two-step method in a volume concentration of 0–1.0 %. Sodium dodecylbenzene sulfonate (SDBS) was used as a stabilizing agent. The TC and VC tested in a 30–60 °C temperature range showed a temperature dependency. A maximum of 14.6 % and 21.9 % enhancement in TC and VC was observed for HNFs compared to the NFs prepared using single NPs. In their study, Kanti et al. [22] investigated the effect of pH on the dispersion stability and thermal properties of CuO and GO-based HNFs in DIW. HNFs were prepared using the standard two-step method in a volume concentration of 0.1–1.0 %, and their TC and VC were tested in a temperature range of 30–60 °C. The NPs ratio in the GO/CuO-based NFs was 50:50 and 20:80, respectively. The former HNFs with higher GO concentration showed enhanced TC compared to the latter with relatively higher concentrations of CuO NPs. This fact might be due to the high TC of GO NPs compared to the CuO NPs and their dominance in the host BFs. Their study used SDBS and Polyvinyl pyrrolidone (PVP) as stabilizing agents. In another similar study [23] with the GO-based HNFs combined with SiO_2 and TiO_2 in DW, the authors investigated the TC and VC of the HNFs in a temperature range of 30–60 °C and volume concentration of NPs 0.05–1.0 %. The concentration of each NPs was 50:50 in ratio with the accompanying NPs. PVP was used as a stabilizing agent, and it was observed PVP has reasonably enhanced the stability of the NFs. It was observed that HNFs showed minor enhancement in the VC compared to the pure GO-based NFs, with a little compromise over the TC of the HNFs. It was emphasized from the study that HNFs are an excellent option as high thermal and cost-effective fluid for high heat flux thermal applications. Wanatasanappan [24], in their study, investigated the rheological behavior of Al_2O_3–Fe_2O_3-based NPs dispersed in a DW-EG mixture. The HNFs were prepared in a DW/EG ratio of 60/40 and 40/60, respectively, and the VC was tested in a temperature range of 0–100 °C. It was confirmed from the investigation that an increase in the concentration of EG in the HNFs has an increasing effect on the VC of the HNFs and vice versa. Also, there was a reduction in VC with the temperature rise, and an overall 87.2 % reduction in VC was observed over a temperature range of 0–100 °C. The experimental findings confirmed the Newtonian behavior of the HNFs. In their other study, Kanti et al. [25] investigated the dispersion stability and thermophysical properties of water-based alumina and graphene oxide-based NFs and their hybrid at varying

mixing ratios. Pure GO-based NFs were observed to have 43.9 % higher TC than the Al_2O_3-based NFs. In GO-Al_2O_3 HNFs, an increase in the concentration of the GO NPs showed an increasing trend in the TC, most probably due to the dominating thermal characteristics of the GO NPs over the Al_2O_3-based NPs. This also shows that the NP's TC plays a vital role in enriching the overall thermal conductivity of the HNFs.

Metallic oxide-based NPs have become very interesting due to their superior thermos-physical properties. ZnO, MgO, Al_2O_3, CuO, and TiO_2-based NPs have been analyzed as the best materials for heat transfer applications. The literature showed that most studies are concerned with the Al_2O_3-based NFs for their thermal performance, probably due to their better dispersion stability in the host BFs [26]. Water and EG are the commonly used heat transfer fluids, and the research investigations confirmed that the aqueous-based HNFs are more suitable than the others prepared in different host BFs. However, the choice of the hybrid BFs is also strongly connected with the nature of thermal application. The aforementioned studies showed that HNFs prepared in different BFs can potentially enhance the heat transfer performance of industrial heat exchange applications [27]. The TC of the HNFs is the prime factor in assessing the thermal efficacy of the HNFs for industrial and commercial applications. Researchers have used different experimental and numerical techniques to investigate this enhancement with the standard operating conditions [28]. The simulation-based methods are proven to be correct in predicting the TC of the HNFs with greater accuracy, hence reducing laboratory costs and saving time [29].

The literature surge also showed extensive research on Al_2O_3, CuO, SiO_2, and TiO_2-based NFs and their hybrids. However, fewer studies have been reported using ZnO and MgO-based HNFs for potential heat transfer and optical application. In contrast, the TC of ZnO and MgO-based NPs is far better than the other metal oxide-based NPs. Also, the dispersion stability of these NPs in the host BFs is reported to be better due to their lower density. The NPs of MgO and ZnO showed distinct chemical and physical properties, and their NFs have been used as cooling fluids in heat transfer devices and optical devices due to the wide band gap. These materials are efficient, thermally reliable, economical, and non-toxic to human health [30]. The thermal performance of the host BFs is also very important when the NFs are to be used for potential heat transfer applications. The studies reporting the dispersions of ZnO and MgO-based HNFs in various host BFs are also lacking. Also, the stability of the prepared HNFs is of prime importance, and the existing literature lacks methods for preparing HNFs with long-lasting dispersion stability [31]. The present research aims to prepare stable ZnO–MgO-based HNFs using plasma synthesis techniques in various BFs consisting of pristine coolant, engine oil, DW, and coconut oil. This study aims to evaluate the optical and thermal properties of the prepared HNFs in the aforementioned BFs to evaluate their potential for various heat transfer and optical applications. The study also intends to ensure the suitability of the considered BFs used while integrating them with the aforementioned NPs. This will add a new data set in the literature on the HNFs utilizing a range of BFs for potential optical and heat transfer applications.

2. Materials and methods

ZnO and MgO NPs with 99.99% purity, as well as the host BFs, i.e., coolant (Anti-Freeze), engine oil (SAE 20W-50), distilled water (DW) and pure coconut oil (parachute), were purchased from the local market. The size of the NPs was estimated using scanning electron microscopy (SEM), as shown in Fig. 1(a) and (b). The ZnO NPs were found to be nearly spherical, and the average size of the NPs ranged between 30 and 60 nm, while the MgO NPs were found in a slack shape, most probably due to the aggregation of the NPs in dry form during storage and transportation.

However, such aggregates are supposed to be broken down in the original size when dispersed in the host BFs to formulate the NFs. At higher magnifications, the SEM images showed the average size distribution of MgO NPs between 20 and 60 nm. ZnO and MgO NPs (50%–50%) in mass concentration were mixed using ball milling for fine mixing and grinding. A hydraulic press machine was used to make the pallet, which was of 5.0 mm thickness. The thermophysical properties of ZnO and MgO NPs, comprising thermal conductivity, specific heat capacity, and true density, are shown in Table 1.

Different BFs comprising coolant, engine oil, DW, and coconut oil used to prepare HNFs in this study are presented in Fig. 2(a–d).

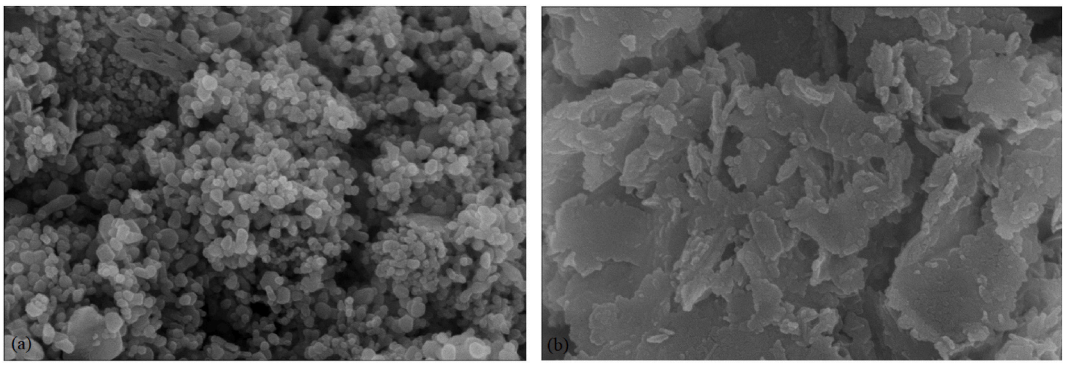

Fig. 1. SEM images of (a) ZnO NPs, (b) MgO NPs.

Table 1
Thermophysical properties of ZnO and MgO NPs.

Properties	Units	ZnO	Reference	MgO	Reference
Color	–	White	–	White	–
Thermal Conductivity	$Wm^{-1}K^{-1}$	29	[32]	48	[33]
Specific Heat Capacity	$Jkg^{-1}K^{-1}$	514	[34]	852	[35]
True Density	Kgm^{-3}	5606	[36]	3580	[37]

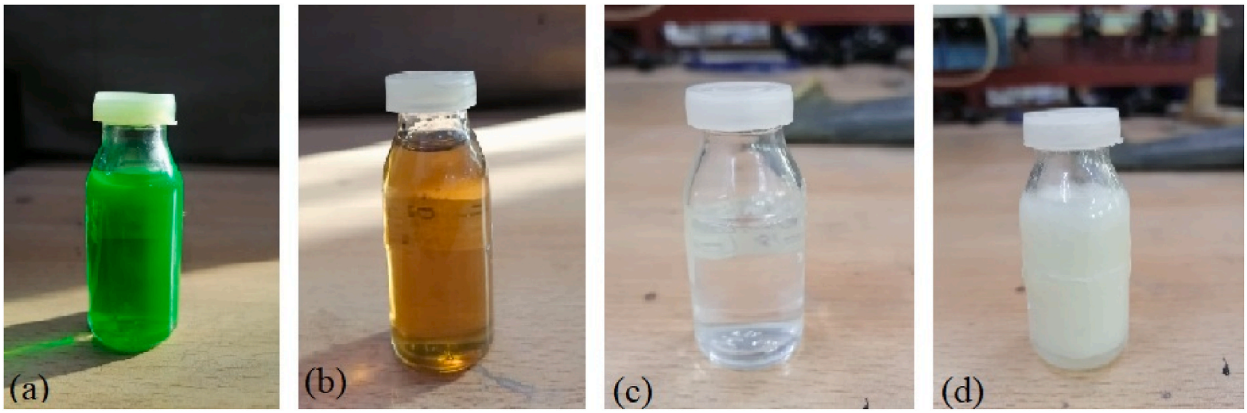

Fig. 2. BFs used for the preparation of HNFs (a) coolant, (b) engine oil, (c) distilled water, (d) coconut oil.

3. Experimental test setup and methods

This section deals with but is not limited to the experimental setups and procedures used to prepare the HNFs and the characterization of NPs and HNFs, including their optical and thermal properties under various operating conditions.

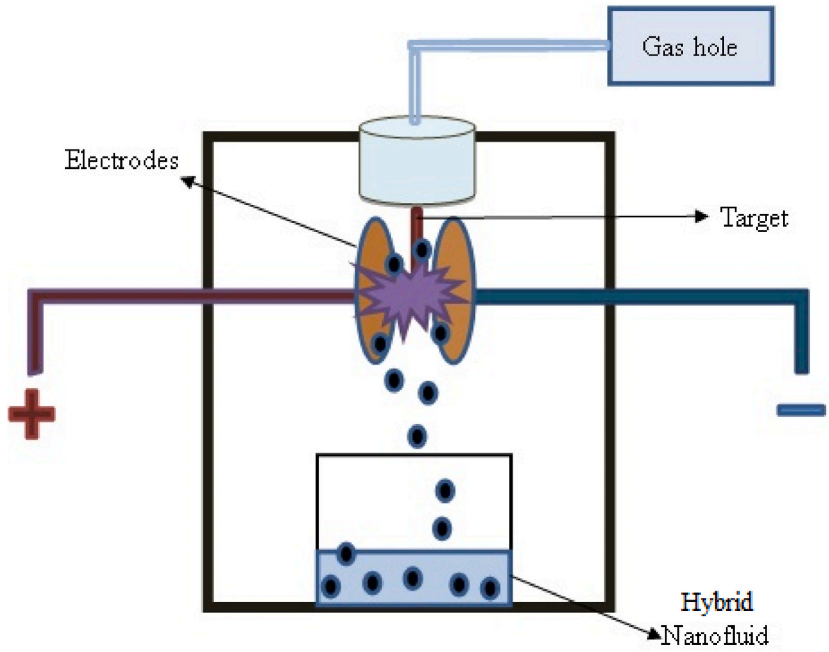

Fig. 3. Schematic of plasma synthesis of ZnO/MgO-based HNFs.

3.1. Plasma synthesis of HNFs

Plasma synthesis is an increasingly popular method for producing NPs through a plasma discharge. The process is initiated by applying a high voltage or electromagnetic field to a gas or liquid, which generates a plasma. The process involves using a plasma torch to vaporize and ionize the two materials, which then react to form NPs dispersed in the liquid [38]. Plasma synthesis is considered a green approach to NPs production because it produces no toxic chemicals or oxidants to human health [39]. In addition to being a safer method of NPs production, plasma synthesis is also a cost-effective and straightforward procedure that eliminates the need for waste handling or post-purification. This is because the process is carried out in a closed system, meaning that the NPs are generated in situ and do not require additional purification steps. Plasma synthesis is highly versatile and can be applied to various nanomaterials, including metals, metal oxides, and carbides. This makes it an attractive option for researchers looking to produce a range of nanomaterials for various applications. Overall, plasma synthesis is a promising method for producing NPs and NFs that is both safe and environmentally friendly [40]. In the present research investigation, HNFs in different BFs were prepared using the plasma synthesis method, a single step, a green chemistry approach, and a cost-effective method. The experimental setup comprised two identical copper electrodes, a sample holder, a gas hole, and a fluid holder, as shown in Fig. 3. The copper electrodes were connected to a high-power supply to generate plasma, and a fluid container was used to collect the NPs.

HNFs in different volume concentrations of 0.019 % for DW, 0.020 % for coolant, 0.016 % for engine oil, and 0.017 % for coconut oil were prepared for their thermal and optical analysis. This approach offers versatility and flexibility in designing experiments. The choice to explore varying NPs concentrations reflects the versatility and adaptability of the experimental design. This flexibility allows researchers to investigate a wide spectrum of NPs loadings, accommodating the complexity of real-world applications where different concentrations may be more suitable. The advantages of plasma synthesis of HNFs include the ability to create NPs of uniform size and shape and the ability to control the composition and properties of the NPs. Additionally, the process is relatively fast and can be performed at room temperature, which is useful for preserving the properties of temperature-sensitive materials [41]. Fig. 4(a–d) shows the whole setup during experimentation, where a high voltage was given to the electrodes to produce plasma. After condensing, the generated plasma interacted with a pallet of ZnO and MgO to produce tiny NPs collected in fluid containers named HNFs. Four different kinds of BFs (DW, coolant, engine oil, and coconut oil) were used to prepare HNFs. Plasma was generated at 8.0 KeV, and the pallet was exposed to plasma for 30 min for every fluid. The collected NPs in BFs were then investigated using different techniques to evaluate their properties.

One of the key challenges in plasma synthesis of HNFs is controlling the size and distribution of the NPs. The size and shape of the NPs can be controlled by adjusting the plasma conditions and the reactant concentrations, but achieving a narrow size distribution can be difficult. Additionally, the stability of the NPs in the liquid can be a concern, as the NPs can agglomerate and form larger NPs over time. However, prepared HNFs were visually inspected for their dispersion stability in the present research study. The observations revealed no measurable signs of aggregation and sedimentation of the NPs within the host BFs for 30 days. This shows that the prepared HNFs possessed reasonably good stability over time and can be used in thermal and optical applications without the concern of sedimentation and aggregation of NPs, which can lead to the clogging of the operating systems.

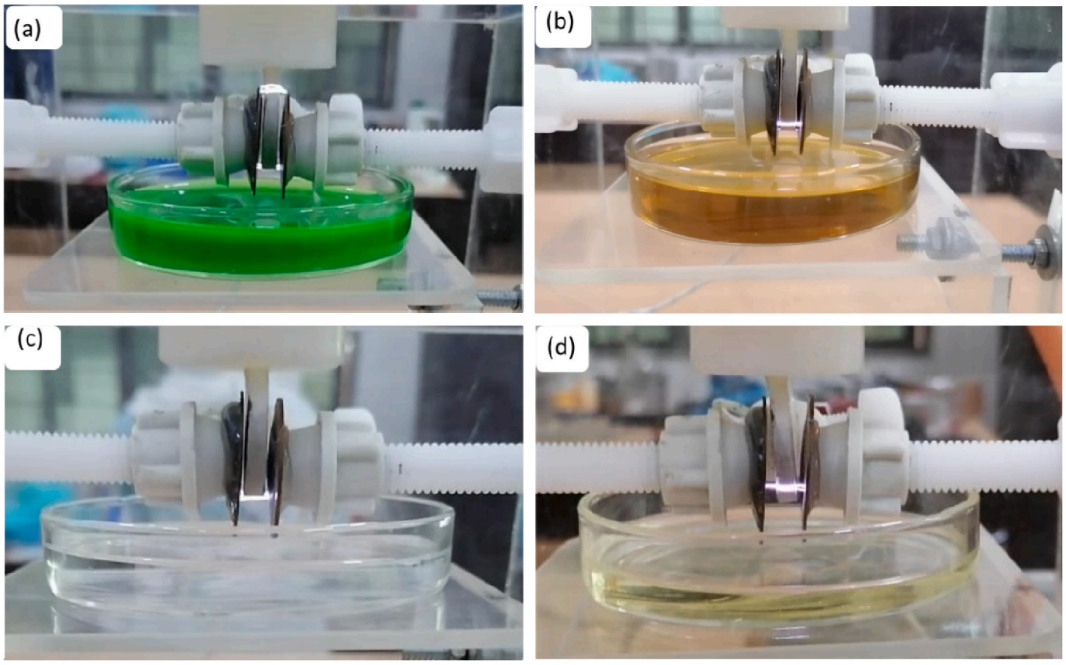

Fig. 4. Images during experimentation; (a) coolant (b) engine oil (c) distilled water (d) coconut oil.

3.2. XRD analysis of NPs

X-ray diffraction (XRD) analysis is a common technique used to characterize the crystal structure of NPs. XRD is based on the principle that X-rays are diffracted by the atoms in a crystal lattice, producing a characteristic diffraction pattern that can be used to identify the crystal structure. When X-rays are directed at a crystal, they are scattered in different directions by the atoms in the crystal lattice. By measuring the angles and intensities of the scattered X-rays, information about the crystal structure, including the positions of atoms in the lattice, can be obtained [42]. In the present investigation, Bruker D8 XRD was used. This analysis showed the crystal structure of NPs of ZnO along with MgO. The XRD technique involves several components, including an X-ray source, a monochromator, a sample holder, and a detector to measure the scattered X-rays. The sample is typically a crystalline powder or a thin film, and it is mounted on the sample holder and exposed to the X-rays. The detector measures the intensity of the scattered X-rays as a function of the scattering angle, which can then be analyzed to determine the crystal structure.

3.3. UV-visible spectroscopy of HNFs

Ultraviolet-visible (UV-Vis) spectroscopy is a common technique used to study the optical properties of NPs. When NPs are exposed to UV or visible light, they absorb certain wavelengths of light depending on their size, shape, and composition. By measuring the absorption spectrum of the NPs, information about their optical properties can be obtained. HNFs are typically composed of NPs dispersed in a liquid medium, and the presence of the NPs can affect the absorption and scattering of light in the UV-visible range [42]. UV-Vis. Spectroscopy involves passing light of different wavelengths through a sample containing the NPs and measuring the amount of absorbed light. The amount of light absorbed is related to the concentration of NPs and the extinction coefficient of the NPs at that wavelength. The extinction coefficient measures how strongly the NPs absorb light at a given wavelength and depends on the NP's size, shape, and composition. The optical properties of HNFs were studied using an Agilent Cary 60 UV-Vis spectrophotometer. A 200–800 nm wavelength was used to scan samples to analyze the absorption. The band gap was calculated from the UV-visible data through the Tauc plot as presented in *Equation (1)* [43],

$$\boldsymbol{\alpha} h\nu = A\left(h\nu - E_g\right)^n \tag{1}$$

where $\boldsymbol{\alpha}$, h, and $\boldsymbol{\nu}$ define the absorption coefficient while E_g is the energy band gap. *h* is called the plank's constant, and *n* shows the direct or indirect transition, and its value is ½ and 2 for indirect and direct band gap materials.

3.4. Thermal conductivity estimation of HNFs

The present experimental investigation examined the TC of ZnO and MgO dispersed in four types of BFs (DW, engine oil, coconut oil, and coolant) based HNFs using a unique TC analyzer (TEMPOS, Meter Group, USA). TEMPOS is a TC analyzer commonly used for measuring the TC of fluids and materials, including NFs and HNFs. A stainless-steel sensor (KS-3) is used to simultaneously apply a small amount of heat in the HNFs to investigate the TC by estimating the heat conduction capability of the HNFs. The sensor simultaneously acts as a heat source and sensor and has a measuring TC range of 0.02–2 W/m.K. The calibration of the sensor using a standard glycerin solution showed experimental accuracy of the instrument within ±1.0 % [44]. A set of 4–6 experimental readings was recorded for accurate thermal conductivity measurement, and then, finally, an average of all the readings was used for final analysis. All the measurements were recorded under controlled temperature conditions within 20–60 °C. One advantage of using TEMPOS to measure the TC of HNFs is its ability to measure small sample volumes. This is important when working with expensive or limited amounts of HNFs. Additionally, TEMPOS can measure the TC of HNFs over a wide temperature range, making it useful for studying the temperature-dependent thermal conductivity of HNFs. However, it is important to note that TEMPOS measurements are affected by various factors, including the fluid's viscosity and density, the fluid film's thickness, and the contact resistance between the fluid and the sensor. Careful calibration and control of these factors are necessary to obtain accurate thermal conductivity measurements using TEMPOS. Table 2 enlists the detailed specifications of all the instruments used in this study.

Table 2
Specifications of typical instruments used for the preparation and characterization of NPs and HNFs.

Name	Model	Specifications
Scanning Electron Microscope	Nova NanoSEM 450	Resolution: 0.8 nm @ 30 kV (STEM), 1.0 nm @ 15 kV (TLD-SE), 1.4 nm @ 1 kV (TLD-SE) and 4.0 nm @ 100 V (CBS)
X-ray diffractometer	Bruker Phaser, Germany Model-D8	Source: Water-cooled sealed X-ray tube; Available anodes: Cr, Cu, Mo, Ag; Detector: LYNXEYE XE-T: Energy resolution <380 eV @ 8 KeV, 0-D, 1-D, 2-D mode; D8 Goniometer: Two-circle
Analytical Balance	AWU-220D Shimadzu	Measuring capacity: 0–82 g, Minimum display: 0.01 mg, response time: 3–15 s, standard deviation: ≤0.1 mg.
Thermal Bath	TC-550MX	Temperature range: −20 °C to +135 °C, Temperature stability: 0.07 °C, Flow rate: 12 LPM, Reservoir capacity: 7.0 L.
UV Vis. Spectrometer	Agilent Cary 60, Agilent	Wavelength range: 190–1100 nm, Spectral bandwidth: 1.5 nm, Wavelength accuracy: ±0.3 nm, Photometric range: −4 to 4 Abs. (double beam); Maximum scanning speed: 24,000 nm/min;
Thermal Conductivity Analyzer	TEMPOS	Accuracy: ±10%, Sensor operating range: −50 to 150 °C, TC range: 0.02–2.0 W/m.K, Sensor needle length/diameter: 6 cm/1.3 mm,

3.5. Mathematical modeling

For the preparation of HNFs, the required amount of material was added to the BFs, and *Equation (2)* was used to measure the percentage volume concentration of the NPs [23]. The volume concentration was 0.019% for water-based HNFs, while for coolant, engine oil, and coconut oil-based HNFs, it turned out to be 0.020 %, 0.016 %, and 0.017 %, respectively.

$$\Phi = \frac{[w/\rho]_{ZnO} + [w/\rho]_{MgO}}{[w/\rho]_{ZnO} + [w/\rho]_{MgO} + [w/\rho]_{bf}} \times 100 \tag{2}$$

Some existing co-relations have been used in this study to compare the experimental results with already proposed experimental models from the literature. A comparison has been made to analyze the authenticity of the conducted results.

$$k_{hnf} = (0.0008794)\varphi_{hnf}^{0.5899} T^{1.345} + 1)k_{bf} \tag{3}$$

$$k_{hnf} = (0.0.0017)\varphi_{hnf}^{0.698} T^{1.396} + 0.981)k_{bf} \tag{4}$$

$$k_{hnf} = 1.024 + 0.5988\varphi_{hnf}^{0.6029} e\left(\frac{\varphi_{hnf}}{T}\right) - \left(\frac{8.059\varphi_{hnf} T^{0.2} + 2.24}{6.052\varphi_{hnf}^{2} + T}\right)k_{bf} \tag{5}$$

Equation (3) [45] and *(4)* [46] present the Esfahani and Kakavandi models, respectively, while *Equation (5)* shows the Esfi model [47] used in the present research investigation.

4. Results and discussion

This section comprises the research results investigated for the characterization of the NPs, the optical properties of the NFs, and the thermal conductivity of ZnO and MgO-based HNFs in the known concentrations of NPs at different operating temperatures.

4.1. XRD analysis of NPs

The X-ray diffraction pattern of MgO–ZnO HNFs (coolant) has been shown in Fig. 5(a), showing the material's crystallinity and

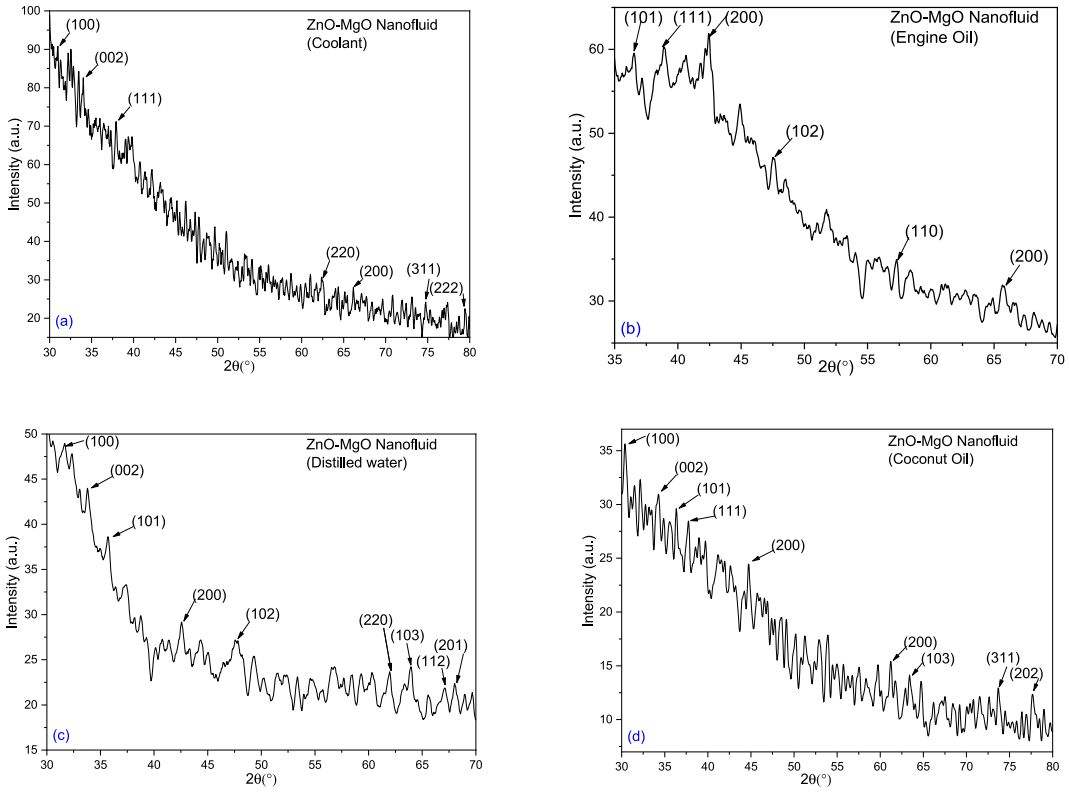

Fig. 5. XRD results of (a) coolant-based HNFs, (b) engine oil-based HNFs, (c) DW-based HNFs, (d) coconut oil-based HNFs.

purity. XRD graph indicates the hexagonal structure of ZnO with the cubic structure of MgO NPs. The peaks in the X-ray diffraction pattern of ZnO at diffraction angles of 31°, 34°, and 66.16° correspond to (100), (002), and (200) crystal planes, respectively. This is according to the JCPDS card no. 00-001-1136, the database for the X-ray diffraction patterns for known materials [48]. MgO peaks show planes (111), (220), (311), and (222) at diffraction angles 37.92°, 62.4°, 74.76° and 79.44° respectively (JCPDS card no. 00-001-1235) [49]. XRD of engine oil having NPs of ZnO and MgO, shown in Fig. 5(b), indicates the materials' pure structure. The resulting peaks are matched with the JCPDS card no. 00-001-1136 of ZnO and JCPDS card N: 00-001-1235 of MgO, which shows the hexagonal structure of the NPs. The peaks at $2\theta = 36.52$, 47.52, 57.28, and 65.68 belong to (101), (102), (110) and (200) planes for ZnO NPs. For MgO NPs, the peaks at $2\theta = 38.88°$ and 42.44° correspond to (111) and (200) planes. NFs of distilled water undergo an X-ray diffraction technique to identify the material structure, as shown in Fig. 5(c).

The resulting peaks of ZnO at diffraction angles 31.68°, 33.8°, 35.72°, 47.56°, 63.96°, 67.12°, 68.04° belong to (100), (002), (101), (102), (103), (112) and (201) planes (JCPDS card no. 00-001-1136). At diffraction angles 42.56° and 61.96°, the planes are (200) and (220) for MgO (JCPDS card no. 00-001 1235). These peaks show the purity and crystallinity of NPs and give the hexagonal structure of NPs. The peaks obtained from the XRD pattern of coconut oil HNFs are presented in Fig. 5(d), which exhibited the peaks of ZnO at $2\theta =$ 30.4°, 34.28°, 36.36°, 63.4°, 77.64° belonging to planes (100), (002), (101), (103) and (202) (JCPDS card no. 00-001-1136). In the case of MgO, the peaks at diffraction angles 37.76°, 44.72°, 61.2°, and 73.68° relate to (111), (200), (220) and (311) planes (JCPDS card no. 00-001-1235). The XRD pattern shows the purity and hexagonal structure of the material.

4.2. UV-visible spectroscopy of HNFs

In Fig. 6(a) and (b), the absorption spectra elucidate the optical characteristics of both coolant and engine oil and their associated HNFs. The absorption spectra of coolant and its HNFs did not show an observable change between them. This suggests that introducing the NPs within the host BFs did not significantly alter the optical properties of the HNFs. Another possible reason is the aggregation of the NPs within the host BFs under strong van der Waals forces and electrostatic interactions; however, this cause is less likely as all the prepared HNFs were visually stable. In conclusion, the consistency observed in the absorption spectra between the coolant and its HNFs suggests that the optical properties of the HNFs in this study are closely aligned with those of the base coolant. This finding highlights the complexity of HNFs behavior and emphasizes the importance of careful characterization and stability assessment when designing and using HNFs for various engineering applications. Further investigations may provide deeper insights into the interplay between NPs, additives, and fluid properties in HNFs systems.

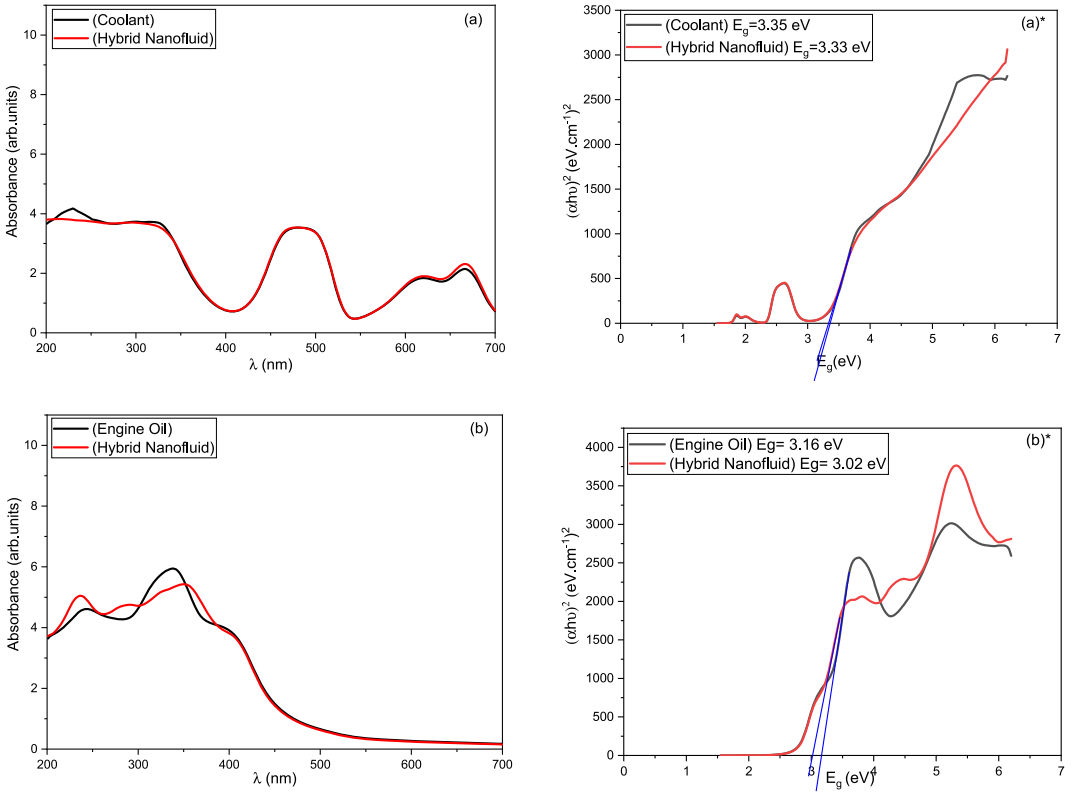

Fig. 6. UV-Vis (a) absorption spectra of coolant and its HNFs (a*) band gap of coolant and its HNFs, (b) absorption spectra of engine oil and its HNFs (b*) band gap of engine oil and its HNFs.

Determining band gaps in materials is fundamental to understanding their electronic properties. In this study, the band gap calculated for the coolant, comprising DW, EG, and additives, was approximately 3.35 eV, as shown in Fig. 6(a)*. This value represents the energy difference between the valence and conduction bands in the coolant, providing a measure of its electrical and optical behavior. Interestingly, when ZnO–MgO NPs were introduced into the coolant, the band gap was slightly reduced to 3.33 eV. This marginal change indicates that these NPs did not significantly alter the electronic structure of the HNFs. It's worth noting that this outcome may be attributed to factors such as particle size, concentration, and dispersion within the HNFs. Observing a red shift in the absorption spectra of engine oil-based HNFs is a noteworthy finding, as presented in Fig. 6(b)*. A red shift implies that the absorption peaks shifted towards longer wavelengths than the BFs. This phenomenon is often associated with changes in the size, shape, or concentration of NPs within the NFs. Surface Plasmon Resonance (SPR) is a potential explanation for this redshift. A sharp absorption peak characterizes SPR due to collective oscillations of electrons on the surface of metallic NPs. Variations in SPR can be indicative of alterations in NPs properties.

DW exhibited absorption spectra in the ultraviolet (UV) region, ranging from a wavelength of 260 nm–295 nm, as illustrated in Fig. 7(a). At the same time, the DW calculated band gap was approximately 3.79 eV, as shown in Fig. 7(a)*. The presence of absorption in the UV region signifies the ability of water to absorb light in this specific wavelength range. Conversely, coconut oil demonstrated a blue shift in its absorption spectra within the UV region, as shown in Fig. 7(b). A blue shift indicates that the absorption peaks shifted towards shorter wavelengths. This shift can be attributed to changes in the nanofluid's composition, size, or dispersion of NPs. Moreover, the band gap of coconut oil increased when NPs were incorporated into the fluid, reaching 4.05 eV in the HNFs compared to 3.95 eV in pure coconut oil, as illustrated in Fig. 7(b)*. This change underscores the impact of NPs on the electronic structure of the fluid and suggests potential applications in modifying its optical properties. The notable wide band gaps observed in the absorption spectra of DW and engine oil HNFs are attributed to the quantum confinement effect. This effect becomes prominent when particles, in this case, NPs, are very small. It causes a widening of the band gap due to the confinement of electrons and quantization of energy levels.

As Fig. 7(b*) shows, negative band gap values in UV-visible spectroscopy are attributed to several factors, including Surface plasmon resonance (SPR), Quantum confinement effects, and heterostructure formation. SPR is a phenomenon that occurs when light interacts with free electrons on the surface of a metal NPs. This can lead to the absorption of light energy and the generation of surface plasmons, which are collective oscillations of the free electrons. SPR can lead to negative band gap values in UV-visible spectroscopy results because the surface plasmons can absorb light energy at wavelengths below the metal NP's band gap. Quantum confinement effects occur when the dimensions of a material are reduced to the nanoscale. This can lead to changes in the electronic band structure

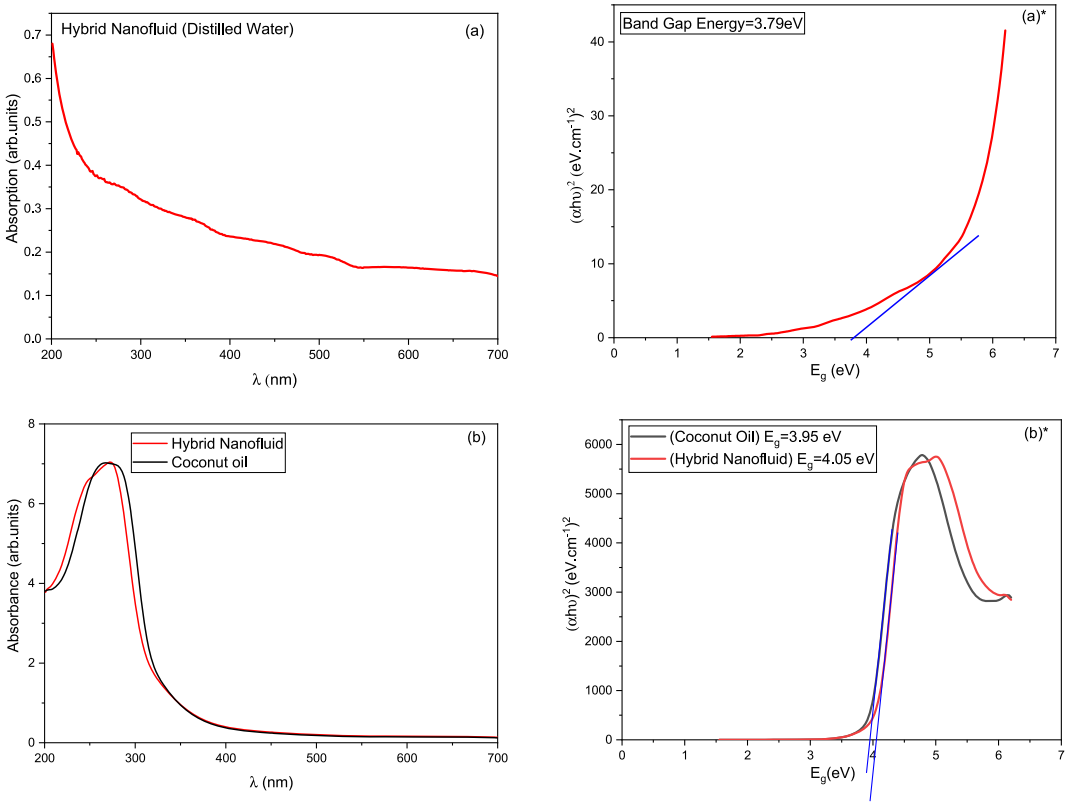

Fig. 7. UV-Vis (a) absorption spectra of DW and its HNFs, (a*) band gap of DW and its HNFs, (b) absorption spectra of coconut oil and its HNFs, (b*) band gap of coconut oil and its HNFs.

of the material, including the band gap.

In some cases, quantum confinement effects can lead to a decrease in the band gap of a material, which can result in negative band gap values in UV-visible spectroscopy results. Heterostructure formation occurs when combining two or more materials to form a single structure. This can lead to the formation of new energy levels at the interface between the two materials.

In some cases, these new energy levels can be below the band gap of the individual materials, resulting in negative band gap values in UV-visible spectroscopy results. The physical meaning of negative band gap values in UV-visible spectroscopy results is that the HNFs can absorb light energy at wavelengths below the band gap of the individual components of the HNFs. This can lead to several interesting properties, such as generating photocurrent without an external bias. It is important to note that negative band gap values in UV-visible spectroscopy results do not necessarily mean that the HNFs have a true band gap below zero. In some cases, the negative band gap values can be an artifact of the measurement technique. However, growing evidence suggests that some hybrid HNFs have true band gap values below zero.

In summary, analyzing band gaps and shifts in absorption spectra in these fluids and their HNFs counterparts provides a deeper understanding of their electronic and optical characteristics. These findings have implications for engineering applications, where the

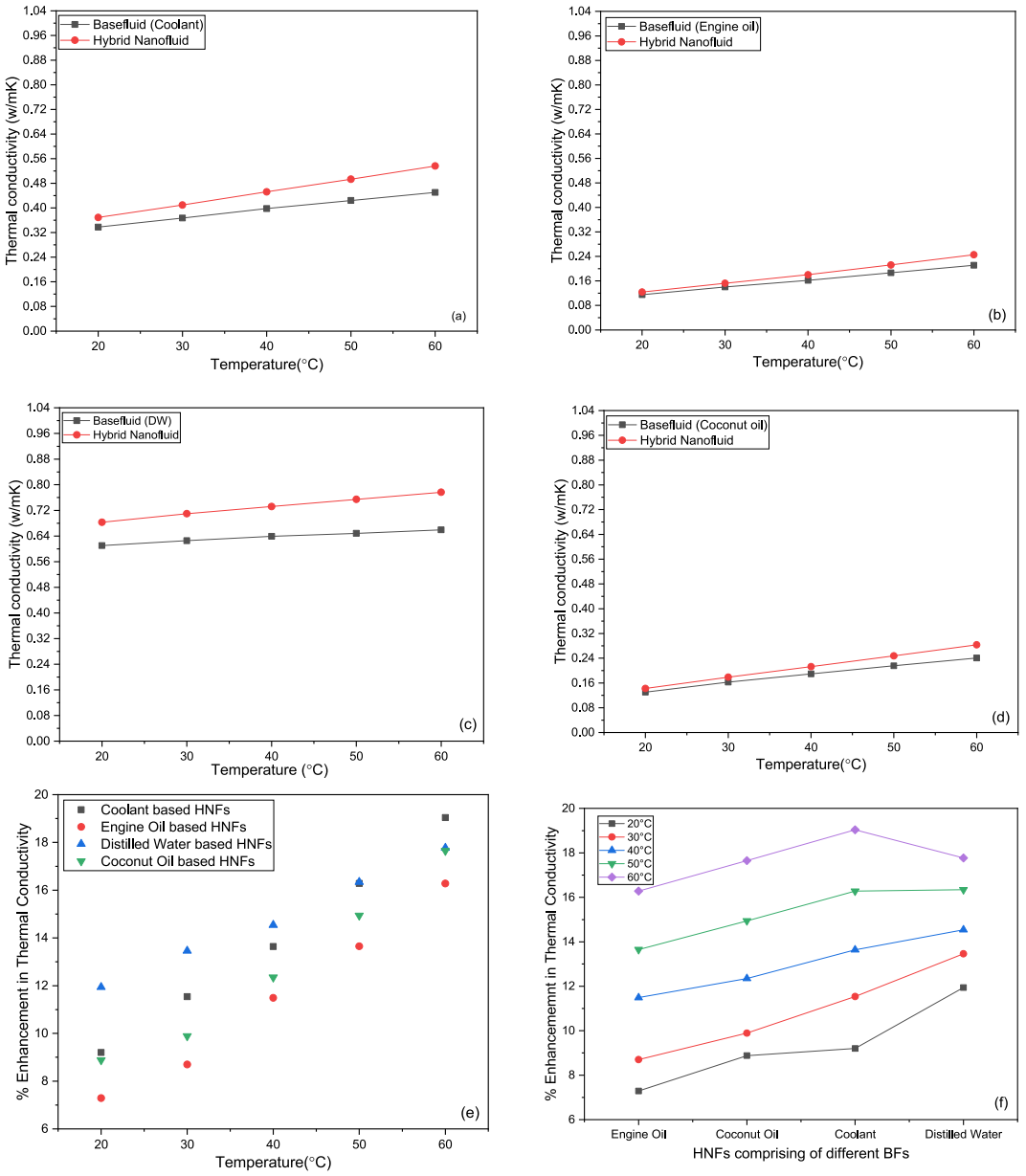

Fig. 8. Thermal conductivity results of HNFs in (a) coolant, (b) engine oil, (c) DW, (d) coconut oil, (e) comparing TC of HNFs, (f) analyzing the effect of temperature on the TC of all HNFs.

optical properties of HNFs can be harnessed to optimize performance in areas such as heat transfer and energy conversion. Further research may explore the precise mechanisms behind these observations and their practical applications.

4.3. Thermal conductivity estimation of HNFs

In this study, the effect of temperature on the thermal conductivity of HNFs was systematically explored by varying the temperature range from 20 to 60 °C, as presented in Fig. 8(a–f). The black line shows the TC of BFs, while the red line shows the thermal conductivity of the HNFs. The obtained results of the thermal conductivity of both fluids were compared, and both showed enhancement in TC with an increment in temperature. Results showed effective enhancement in the thermal conductivity of HNFs compared to the BFs, and with greater temperature value, this increment is more prominent. This temperature-dependent analysis offers valuable information regarding these fluids' heat transfer characteristics and potential applications. A significant outcome of this investigation was the effective enhancement in the thermal conductivity of NFs compared to their respective BFs. This enhancement became more pronounced with higher temperatures. The enhanced thermal conductivity in HNFs is valuable for various heat transfer applications, implying improved heat dissipation and transfer efficiency. One possible explanation for the observed enhancement in thermal conductivity with increasing temperature is the heightened Brownian motion of NPs within the NFs. The system's thermal energy increases as the temperature rises, leading to greater particle movement.

This enhanced particle motion improves heat transfer by promoting more efficient interactions between the NPs and the basefluid. A percentage increment of 9.2 %–19.04 % was observed in the case of coolant-based HNFs from 20 to 60 °C as shown in Fig. 8(a). 7.29 %–16.28 % enhancement in TC was calculated for engine oil-based HNFs, as presented in Fig. 8(b). The enhancement of 11.94 %–17.77 % and 8.88 %–17.65 % were observed in DW and coconut oil-based HNFs, as shown in Fig. 8(c) and (d), respectively. Fig. 8(e) and (f) present the percentage enhancement in the thermal conductivity of the HNFs concerning temperature and host BFs, respectively. Fig. 8(e) shows how the enhancement in the temperature influences the thermal conductivity of the HNFs, and it shows that the thermal conductivity of the HNFs also changes with the nature of the host BFs. In the present study, there is an increasing trend in the thermal conductivity with the rise in temperature of the host BFs.

On the other hand, Fig. 8(f) shows that the nature of the host BFs also influences the thermal performance of the HNFs and may be attributed to the thermal conductivity of the host BFs. It may be observed from Fig. 8(a–f) that the thermal conductivity of the BFs and the corresponding HNFs is not consistent with the temperature, and the rise in thermal conductivity with temperature does not follow

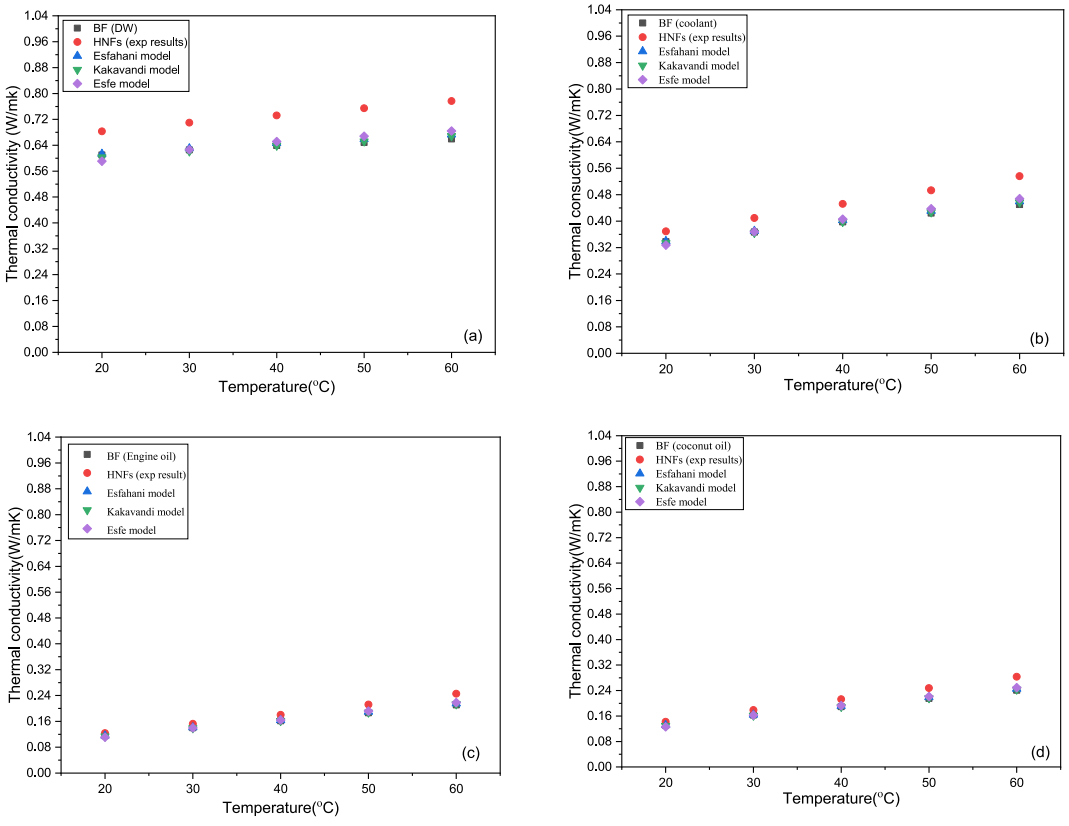

Fig. 9. Comparison of experimental results with proposed models, (a) coolant-based HNFs, (b) engine oil based HNFs, (c) distilled water-based HNFs, (d) coconut oil based HNFs.

the same trend and correlation for both BFs and the corresponding HNFs. There can be many reasons for such kind of abnormalities. The existing literature confirmed that the thermal conductivity of the HNFs depends upon various factors, which include but are not limited to the operating temperature of the NFs, the nature and morphology of the NPs, the type and nature of BFs, the concentration of the NPs, Brownian motion of the NPs within the host BFs, stability of the NPs within the host BFs and last but not the least the purity of the NPs and host BFs. These factors are collectively responsible for any abrupt changes in the thermal conductivity of the HNFs compared with the BFs and show some inconsistent results [50].

The investigation revealed that the maximum enhancement in thermal performance was observed in coolant-based HNFs, followed by DW, coconut oil, and engine oil-based HNFs concerning temperature. This ranking suggests that the choice of base fluid and NPs can significantly influence the extent of enhancement in thermal conductivity. In conclusion, the temperature-dependent thermal conductivity analysis in BFs and HNFs showcased the potential of HNFs for improving heat transfer properties. The observed enhancements, driven by increased temperature and Brownian motion, indicate that HNFs have promising applications in various fields, including electronics cooling, automotive engine cooling, and thermal energy storage. Further research may delve into optimizing nanofluid compositions and exploring practical implementations of these enhanced thermal properties.

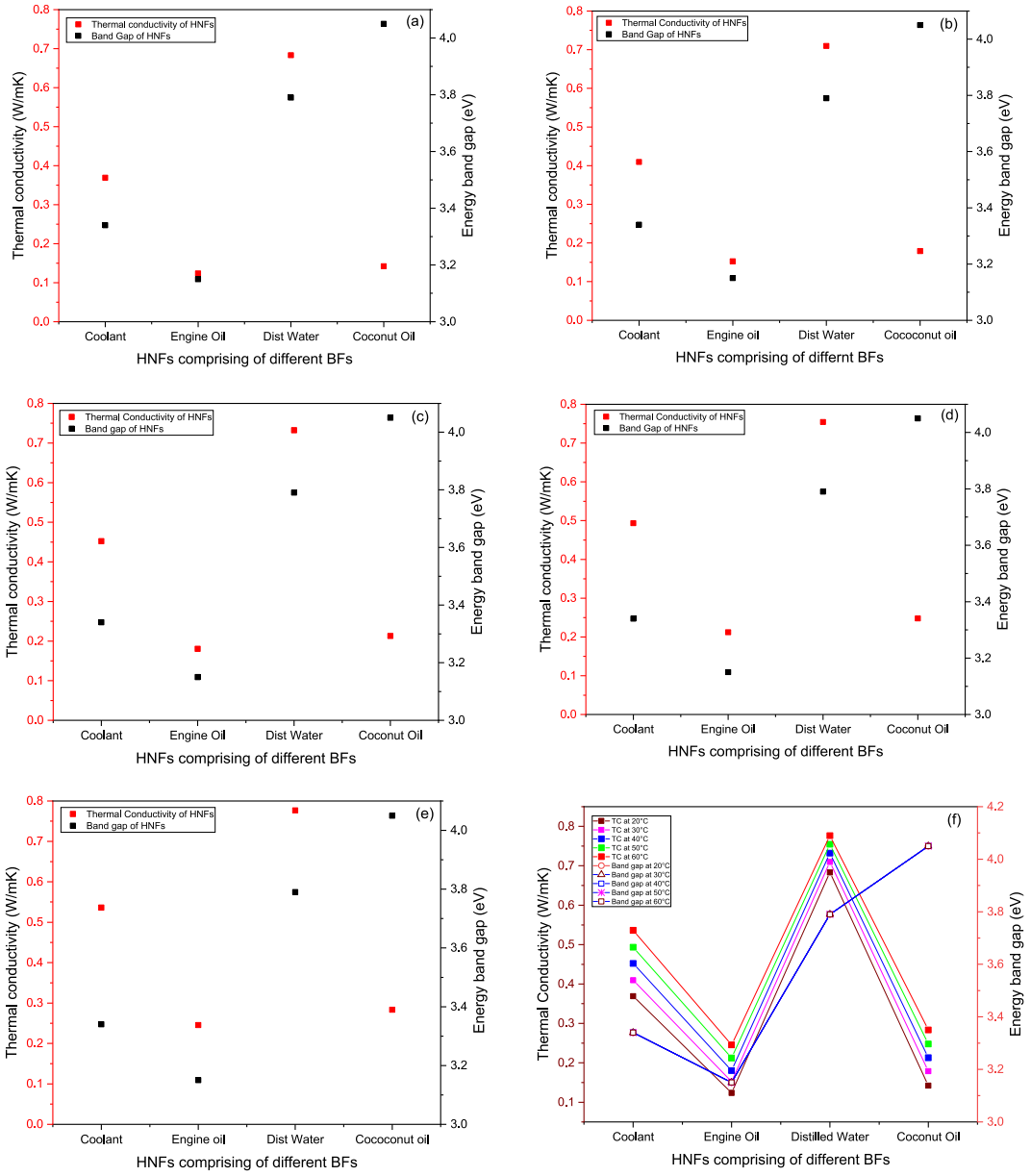

Fig. 10. Comparison of thermal conductivity and band gap of HNFs; (a) at 20 °C (b) at 30 °C (c) at 40 °C (d) at 50 °C (e) at 60 °C (f) Thermal conductivity and band gap under varying temperatures.

4.4. Experimental and theoretical comparison of thermal conductivity

The experimental findings of the present study were compared with existing mathematical models, as presented in Fig. 9. It was observed from the analysis that the results predicted by the existing mathematical models were not in good comparison with the experimental results. The leading cause is that these models have been proposed based on investigations with different natures of NPs, shapes, sizes, concentrations, and operating conditions. Fig. 9(a) shows a considerable difference between the experimental and predicted results from the employed mathematical models. This considerable difference may be attributed to the higher thermal conductivity of the DW compared to other host BFs used in this study. This difference is insignificant for coolant, engine oil, and coconut oil-based HNFs, as presented in Fig. 9(b, c, and d).

Esfahani model [45] was used for ZnO–Ag type of NPs, in 50:50 ratio of NPs concentration in DW. The model was proposed based on the collected experimental data considering only the operating temperature and concentration of NPs. The Kakavandi model [46] was used for MWCNT and SiC NPs dispersed in a binary solution of EG/DW. The model was proposed considering the thermal conductivity in a 25–50 °C temperature range and NPs concentration of 0–0.75 %. Esfe [47] Model was proposed to evaluate the thermal conductivity of ZnO/MWCNT in a binary solution of EG/DW-based HNFs up to 50 °C temperature and volume fraction between 0.02 and 1.0%.

The results presented in Fig. 9 show that the existing models failed to predict the experimental findings with reasonable accuracy. Most of the existing models, along with the models presented in Fig. 9, considered only one or two parameters, e.g., the operating temperature and concentration of the NPs, while the other properties of the NPs, as discussed above such as the nature, morphology, and crystal structures also very important and plays a vital role in thermal performance of the resulting HNFs. The literature surge also revealed that most models are proposed for a specific type and nature of NPs under the standard operating conditions under which the HNFs are subjected. These models are valid for only those specific HNFs and cannot be applied to all HNFs under a wide range of operating conditions [50].

Hence, to thoroughly understand the thermal behavior of the NPs in the host BFs, it is highly necessary to consider all the discussed characteristics of the NPs while developing new models. To investigate the thermal conductivity of ZnO and MgO-based HNFs with different kinds of BFs, new models are needed that focus on the aforementioned properties of the NPs and the properties of the host BFs. The temperature, concentration of NPs, size, and shape should also be considered, as they play a major role in enhancing thermal conductivity.

4.5. Thermal conductivity and band gap analysis of HNFs

Comparison has been made between thermal conductivity and band gap of all different host BFs containing NPs of ZnO and MgO to analyze which HNFs are highly thermally conductive and have a wider band gap, as presented in Fig. 10. This comparison aimed to investigate the HNFs with a wider band gap and higher thermal conductivity. The analysis was performed at a temperature of 20–60 °C, as presented in Fig. 10(a)–(e), respectively. The primary y-axis presents the thermal conductivity with the temperature, while the secondary y-axis presents the energy band gap. The results showed that DW-based HNFs possessed reasonably good thermal and optical properties over the others for potential applications in thermal and optoelectronic devices. From Fig. 10(a)–(e), it can be seen that where the temperature change affected the thermal conductivity of all the HNFs, there was no significant impact on the optical properties of the HNFs with the temperature variation. Fig. 10(f) shows a combined comparative analysis of HNFs for all the considered temperatures. It can be concluded that the ZnO/MgO-based HNFs in DW could be the best alternative to replace conventional BFs-based heat-exchanging fluids. The DW-based HNFs showed comparatively higher thermal conductivity, most probably due to the NPs dispersed in the BFs and the DW's relatively higher thermal conductivity compared to the other BFs.

This fact showed that while preparing the HNFs, the thermal conductivity of the host BFs also plays a vital role in the overall enhancement of the thermal performance and should be considered. Also, the optical properties of the DW-based HNFs are comparatively better than the other HNFs, as the NPs dispersed in the DW are more prone to absorb light than the other BFs.

5. Conclusions and future recommendations

The research outcomes of the present study confirm that the NFs prepared using plasma synthesis techniques are economically viable for producing stable NFs for enhanced heat transfer applications. Enhancement in thermal performance has been detected with the inclusion of NPs into the BFs and with increasing temperature. The maximum enhancement in the thermal conductivity of the NFs was observed in coolant-based NFs, which was 9.2 %–19.04 % in the 20–60 °C temperature range, followed by DW that ranges from 11.94 % to 17.77 %. This outcome suggests the potential of coolant-based NFs for high heat flux thermal applications. An enhancement of 8.88 %–17.65 % and 7.29 %–16.28 % were observed in the case of coconut oil and engine oil, respectively, under similar operating conditions. The NFs of DW proved to be a good option for enhanced heat transfer and optical properties. These NFs exhibited a wider band gap in optoelectronics devices, making them a promising choice for such applications. The research findings underscored the significance of NPs size in influencing the band gap. Only very small-sized NPs could improve the band gap, emphasizing the importance of precise control over NPS characteristics. NFs can be considered promising next-generation fluids for heat transfer devices. Their ability to enhance thermal conductivity can potentially revolutionize heat exchange systems in various industries.

It is important to note that while this study provides valuable insights, much more research is needed to fully harness the potential of NFs in modern heat transfer devices. Future work should explore different combinations of NPs, various types of BFs, alternative fabrication methods, and the use of surfactants to address dispersion stability, a critical challenge in the practical implementation of

NFs.

In conclusion, this study establishes a strong foundation for applying plasma-synthesized NFs in heat transfer enhancement. The remarkable improvements in thermal conductivity observed, especially in coolant-based NFs, highlight the promise of these nanofluids for addressing heat transfer challenges in various domains. Further research and innovation are essential to unlock NFs' full potential and overcome the hurdles in their deployment for modern heat transfer applications.

CRediT authorship contribution statement

Aqsa Nazir: Writing – original draft, Methodology, Investigation, Conceptualization. **Adnan Qamar:** Writing – review & editing, Visualization, Validation, Investigation. **Muhammad Shahid Rafique:** Writing – review & editing, Methodology, Investigation, Formal analysis. **Ghulam Murtaza:** Writing – review & editing, Formal analysis. **Tehreem Arshad:** Writing – review & editing, Formal analysis, Data curation. **Abdul Muneeb:** Writing – review & editing, Formal analysis, Data curation. **Kanwal Jabeen:** Writing – review & editing, Software, Data curation. **M.A. Mujtaba:** Writing – review & editing, Software. **H. Fayaz:** Writing – review & editing, Funding acquisition. **C Ahamed Saleel:** Writing – review & editing, Funding acquisition.

Declaration of competing interest

The authors declare that they have no known competing financial interests or personal relationships that could have appeared to influence the work reported in this paper.

Acknowledgement

The authors extend their appreciation to the Deanship of Scientific Research at King Khalid University for funding this work through a small group Research Project under grant number RGP 1/80/44. The authors of the current investigation would like to pay their profound gratitude to the University of Engineering and Technology (UET), Lahore, Pakistan, for the availability of funding and approach to the scientific equipment for the accomplishment of the current research study under Research Grant No. ORIC/105-ASRB/3084, ORIC/101-ASRB/4452 and ORIC/101-ASRB/4453.

Nomenclature

NFs	Nanofluids
BFs	Base fluids
HNFs	Hybrid Nanofluids
NPs	Nanoparticles
TC	Thermal Conductivity (W/m.K)
DW	Distilled Water
EG	Ethylene Glycol
VC	Viscosity
SEM	Scanning Electron Microscope
XRD	X-ray diffraction
T	Temperature (K)
k	Thermal Conductivity (W/m.K)

Greek symbols

Ø	volume fraction (–)
ρ	density (kg/m^3)

Subscripts

bf	base fluid
nf	nanofluid
np	nanoparticle
hnf	hybrid nanofluid

References

[1] M. Bahiraei, S. Heshmatian, Electronics cooling with nanofluids: a critical review, Energy Convers. Manag. 172 (2018) 438–456, https://doi.org/10.1016/j.enconman.2018.07.047. March.

[2] N. Zhao, S. Li, J. Yang, A review on nanofluids: data-driven modeling of thermalphysical properties and the application in automotive radiator, Renew. Sustain. Energy Rev. 66 (2016) 596–616, https://doi.org/10.1016/j.rser.2016.08.029.

[3] N.S. Suhaimi, et al., Optimum electrical and dielectric performance of multi-walled carbon nanotubes doped disposed transformer oil, Energies 13 (12) (2020), https://doi.org/10.3390/en13123181.

[4] Y.H. Hung, W.P. Wang, Y.C. Hsu, T.P. Teng, Performance evaluation of an air-cooled heat exchange system for hybrid nanofluids, Exp. Therm. Fluid Sci. 81 (Feb. 2017) 43–55, https://doi.org/10.1016/j.expthermflusci.2016.10.006.

[5] D.K. Devendiran, V.A. Amirtham, A review on preparation, characterization, properties and applications of nanofluids, Renew. Sustain. Energy Rev. 60 (2016) 21–40, https://doi.org/10.1016/j.rser.2016.01.055.

[6] H. Babar, H.M. Ali, Towards hybrid nanofluids: preparation, thermophysical properties, applications, and challenges, J. Mol. Liq. 281 (2019) 598–633, https://doi.org/10.1016/j.molliq.2019.02.102.

[7] V. Singh, M. Gupta, Heat transfer augmentation in a tube using nanofluids under constant heat flux boundary condition: a review, Energy Convers. Manag. 123 (2016) 290–307, https://doi.org/10.1016/j.enconman.2016.06.035.

[8] S.K. Das, S.U.S. Choi, H.E. Patel, Heat transfer in nanofluids - a review, Heat Tran. Eng. 27 (10) (2006) 3–19, https://doi.org/10.1080/01457630600904593.

[9] N.A.C. Sidik, I.M. Adamu, M.M. Jamil, G.H.R. Kefayati, R. Mamat, G. Najafi, Recent progress on hybrid nanofluids in heat transfer applications: a comprehensive review, Int. Commun. Heat Mass Tran. 78 (2016) 68–79, https://doi.org/10.1016/j.icheatmasstransfer.2016.08.019.

[10] J.A.R. Babu, K.K. Kumar, S.S. Rao, State-of-art review on hybrid nanofluids, Renew. Sustain. Energy Rev. 77 (2017) 551–565, https://doi.org/10.1016/j.rser.2017.04.040 [Online]. Available:.

[11] M.C. Mbambo, et al., Thermal conductivity enhancement in gold decorated graphene nanosheets in ethylene glycol based nanofluid, Sci. Rep. 10 (1) (2020) 1–10, https://doi.org/10.1038/s41598-020-71740-1.

[12] M.H. Hamzah, N.A.C. Sidik, T.L. Ken, R. Mamat, G. Najafi, Factors affecting the performance of hybrid nanofluids: a comprehensive review, Int. J. Heat Mass Tran. 115 (2017) 630–646, https://doi.org/10.1016/j.ijheatmasstransfer.2017.07.021.

[13] P.K. Das, A review based on the effect and mechanism of thermal conductivity of normal nanofluids and hybrid nanofluids, J. Mol. Liq. 240 (2017) 420–446, https://doi.org/10.1016/j.molliq.2017.05.071.

[14] L. Yang, W. Ji, M. Mao, J. nan Huang, An updated review on the properties, fabrication and application of hybrid-nanofluids along with their environmental effects, J. Clean. Prod. 257 (2020), https://doi.org/10.1016/j.jclepro.2020.120408.

[15] A. Qamar, et al., Dispersion stability and rheological characteristics of water and ethylene glycol based ZnO nanofluids, Therm. Sci. 25 (3) (2021) 1989–2001, https://doi.org/10.2298/TSCI200110187Q.

[16] N. Ali, J.A. Teixeira, A. Addali, A review on nanofluids: fabrication, stability, and thermophysical properties, J. Nanomater. 2018 (2018), https://doi.org/10.1155/2018/6978130.

[17] M.S. Kumar, V. Vasu, A.V. Gopal, Thermal conductivity and rheological studies for Cu–Zn hybrid nanofluids with various basefluids, J. Taiwan Inst. Chem. Eng. 66 (2016) 321–327, https://doi.org/10.1016/j.jtice.2016.05.033.

[18] M. Hemmat Esfe, S. Alidoust, D. Toghraie, Comparison of thermal conductivity of water-based nanofluids with various combinations of MWCNT, CuO, and SiO2nanoparticles for using in heating systems, Case Stud. Therm. Eng. 42 (2023) 102683, https://doi.org/10.1016/j.csite.2022.102683. October 2022.

[19] M. Hemmat Esfe, S. Alidoust, S.N. Hosseini Tamrabad, D. Toghraie, H. Hatami, Thermal conductivity of MWCNT-TiO2/Water-EG hybrid nanofluids: calculating the price performance factor (PPF) using statistical and experimental methods (RSM), Case Stud. Therm. Eng. 48 (2023) 103094, https://doi.org/10.1016/j.csite.2023.103094. October 2022.

[20] M. Hemmat Esfe, S. Alidoust, D. Toghraie, Comparison of the thermal conductivity of hybrid nanofluids with a specific proportion ratio of MWCNT and TiO2 nanoparticles based on the price performance factor, Mater. Today Commun. 34 (2023) 105411, https://doi.org/10.1016/j.mtcomm.2023.105411. November 2022.

[21] H.B. Marulasiddeshi, P.K. Kanti, M. Jamei, S.B. Prakash, S.N. Sridhara, Z. Said, Experimental study on the thermal properties of Al2O3-CuO/water hybrid nanofluids: development of an artificial intelligence model, Int. J. Energy Res. 46 (15) (2022) 21066–21083, https://doi.org/10.1002/er.8739.

[22] P. Kumar Kanti, P. Sharma, K.V. Sharma, M.P. Maiya, The effect of pH on stability and thermal performance of graphene oxide and copper oxide hybrid nanofluids for heat transfer applications: application of novel machine learning technique, J. Energy Chem. 82 (2023) 359–374, https://doi.org/10.1016/j.jechem.2023.04.001.

[23] P. Kanti, K.V. Sharma, R.S. Khedkar, T. ur Rehman, Synthesis, characterization, stability, and thermal properties of graphene oxide based hybrid nanofluids for thermal applications: experimental approach, Diam. Relat. Mater. 128 (2022), https://doi.org/10.1016/j.diamond.2022.109265. July.

[24] V. Vicki Wanatasanappan, P. Kumar Kanti, P. Sharma, N. Husna, M.Z. Abdullah, Viscosity and rheological behavior of Al2O3-Fe2O3/water-EG based hybrid nanofluid: a new correlation based on mixture ratio, J. Mol. Liq. 375 (2023), https://doi.org/10.1016/j.molliq.2023.121365.

[25] P.K. Kanti, P. Sharma, M.P. Maiya, K.V. Sharma, The stability and thermophysical properties of Al2O3-graphene oxide hybrid nanofluids for solar energy applications: application of robust autoregressive modern machine learning technique, Sol. Energy Mater. Sol. Cells 253 (2023), https://doi.org/10.1016/j.solmat.2023.112207. July 2022.

[26] M. Hemmat Esfe, S. Esfandeh, M.H. Kamyab, D. Toghraie, Analytical-statistical review of selected researches in the field of thermal conductivity of nanofluids, Powder Technol. 416 (2023) 118195, https://doi.org/10.1016/j.powtec.2022.118195. November 2022.

[27] M.H. Esfe, S. Alidoust, D. Toghraie, Correlation and thermal conductivity sensitivity analysis of ternary hybrid nanofluids containing CuO and TiO2 nanoparticles and multi-walled carbon nanotubes, Kor. J. Chem. Eng. 40 (9) (2023) 2312–2320, https://doi.org/10.1007/s11814-022-1320-z.

[28] M. Hemmat Esfe, S. Esfandeh, D. Toghraie, Investigation of different training function efficiency in modeling thermal conductivity of TiO2/Water nanofluid using artificial neural network, Colloids Surf. A Physicochem. Eng. Asp. 653 (2022) 129811, https://doi.org/10.1016/j.colsurfa.2022.129811. July.

[29] M. Hemmat Esfe, H. Hatami, M. Kiannejad Amiri, S. Alidoust, D. Toghraie, S. Esfandeh, Multi-objective optimization of viscosity and thermal conductivity of TiO2/BioGlycol-water nanofluids with sorting non-dominated genetic algorithm II coupled with response surface methodology, Mater. Today Commun. 36 (2023) 106718, https://doi.org/10.1016/j.mtcomm.2023.106718. May.

[30] R. Vidhya, T. Balakrishnan, B.S. Kumar, Investigation on thermophysical properties and heat transfer performance of heat pipe charged with binary mixture based ZnO-MgO hybrid nanofluids, Mater. Today Proc. 37 (2020) 3423–3433, https://doi.org/10.1016/j.matpr.2020.09.284.

[31] A. Qamar, et al., Preparation and dispersion stability of aqueous metal oxide nanofluids for potential heat transfer applications: a review of experimental studies, J. Therm. Anal. Calorim. 147 (1) (2022) 23–46, https://doi.org/10.1007/s10973-020-10372-z.

[32] F. Asadi, Amin Porrfattah, Heat transfer performance of two oil-based nanofluids containing ZnO and MgO nanoparticles; a comparative experimental investigation, Powder Technol. 343 (2019) 296–308.

[33] P. Rabbani, A. Hamzehpour, M. Ashjaee, M. Najafi, E. Houshfar, Experimental investigation on heat transfer of MgO nanofluid in tubes partially filled with metal foam, Powder Technol. 354 (2019) 734–742, https://doi.org/10.1016/j.powtec.2019.06.037.

[34] T. Wen, L. Lu, H. Zhong, B. Shen, Thermal properties measurement and performance evaluation of water/ZnO nanofluid in a mini channel with offset fins, Int. J. Heat Mass Tran. 162 (2020) 120361, https://doi.org/10.1016/j.ijheatmasstransfer.2020.120361.

[35] S.M. Mousavi, F. Esmaeilzadeh, X.P. Wang, A detailed investigation on the thermo-physical and rheological behavior of MgO/TiO 2 aqueous dual hybrid nanofluid, J. Mol. Liq. 282 (2019) 323–339, https://doi.org/10.1016/j.molliq.2019.02.100.

[36] A. Topuz, T. Engin, A. Alper Özalp, B. Erdoğan, S. Mert, A. Yeter, Experimental investigation of optimum thermal performance and pressure drop of water-based Al2O3, TiO2 and ZnO nanofluids flowing inside a circular microchannel, J. Therm. Anal. Calorim. 131 (2018) 2843–2863, https://doi.org/10.1007/s10973-017-6790-6.

[37] M. Afrand, Experimental study on thermal conductivity of ethylene glycol containing hybrid nano-additives and development of a new correlation, Appl. Therm. Eng. 110 (2017) 1111–1119, https://doi.org/10.1016/j.applthermaleng.2016.09.024.

[38] D. Vollath, Plasma synthesis of nanopowders, J. Nanoparticle Res. 10 (2008) 39–57, https://doi.org/10.1007/s11051-008-9427-7.

[39] N.K. Kaushik, et al., Plasma and nanomaterials: fabrication and biomedical applications, Nanomaterials 9 (1) (2019) 1–19, https://doi.org/10.3390/nano9010098.

[40] I. Chang Dr, Plasma synthesis of metal nanopowders, Adv. Powder Metall. Prop. Process. Appl. (2013) 69–85, https://doi.org/10.1533/9780857098900.1.69.

[41] P.G. Jamkhande, N.W. Ghule, A.H. Bamer, M.G. Kalaskar, Metal nanoparticles synthesis: an overview on methods of preparation, advantages and disadvantages, and applications, J. Drug Deliv. Sci. Technol. 53 (2019) 101174, https://doi.org/10.1016/j.jddst.2019.101174.
[42] C.J. Chirayil, J. Abraham, R.K. Mishra, S.C. George, S. Thomas, Instrumental techniques for the characterization of nanoparticles, in: Thermal and Rheological Measurement Techniques for Nanomaterials Characterization vol. 3, Elsevier Inc., 2017, pp. 1–36, https://doi.org/10.1016/B978-0-323-46139-9.00001-3.
[43] P.R. Jubu, F.K. Yam, V.M. Igba, K.P. Beh, Tauc-plot scale and extrapolation effect on bandgap estimation from UV–vis–NIR data – a case study of β-Ga2O3, J. Solid State Chem. 290 (2020) 1–8, https://doi.org/10.1016/j.jssc.2020.121576. May.
[44] A. Qamar, Z. Anwar, H. Ali, S. Imran, R. Shaukat, M. Mujtaba Abbas, Experimental investigation of dispersion stability and thermophysical properties of ZnO/DIW nanofluids for heat transfer applications, Alex. Eng. J. (2021), https://doi.org/10.1016/j.aej.2021.09.028.
[45] N.N. Esfahani, D. Toghraie, M. Afrand, A new correlation for predicting the thermal conductivity of ZnO–Ag (50%–50%)/water hybrid nanofluid: an experimental study, Powder Technol. 323 (2018) 367–373, https://doi.org/10.1016/j.powtec.2017.10.025.
[46] A. Kakavandi, M. Akbari, Experimental investigation of thermal conductivity of nanofluids containing of hybrid nanoparticles suspended in binary base fluids and propose a new correlation, Int. J. Heat Mass Tran. 124 (2018) 742–751, https://doi.org/10.1016/j.ijheatmasstransfer.2018.03.103.
[47] M. Hemmat Esfe, S. Esfandeh, S. Saedodin, H. Rostamian, Experimental evaluation, sensitivity analyzation and ANN modeling of thermal conductivity of ZnO-MWCNT/EG-water hybrid nanofluid for engineering applications, Appl. Therm. Eng. 125 (2017) 673–685, https://doi.org/10.1016/j.applthermaleng.2017.06.077.
[48] A.H.M. Leung, et al., Layered zinc hydroxide monolayers by hydrolysis of organozincs, Chem. Sci. 9 (8) (2018) 2135–2146, https://doi.org/10.1039/c7sc04256f.
[49] I. Jendrzejewska, Application of X-ray powder diffraction for analysis of selected dietary supplements containing magnesium and calcium, Front. Chem. 8 (2020) 1–12, https://doi.org/10.3389/fchem.2020.00672. September.
[50] M.U. Sajid, H.M. Ali, Thermal conductivity of hybrid nanofluids : a critical review, Int. J. Heat Mass Tran. 126 (2018) 211–234, https://doi.org/10.1016/j.ijheatmasstransfer.2018.05.021 [Online]. Available:.